Functional implications of the structure of the murine parvovirus, minute virus of mice

Mavis Agbandje-McKenna[1†], Antonio L Llamas-Saiz[1‡], Feng Wang[2§], Peter Tattersall[2] and Michael G Rossmann[1*]

Background: Minute virus of mice (MVM) is a single-stranded (ss) DNA-containing, murine parvovirus with a capsid built up of 60 icosahedrally related polypeptide chains, each of which consists of the C-terminal region common to two structural proteins, VP1 and VP2. In infectious virions, most VP2 molecules are cleaved to VP3 by the removal of about 20 amino acids from the N terminus. Of the 587 amino acids in VP2, approximately half are identical to those in the analogous capsid protein of the antigenically distinct canine parvovirus (CPV), the crystal structure of which has previously been determined. The three-dimensional structure determination of MVMi (the immunosuppressive strain of MVM) was previously reported to 3.5 Å resolution.

Results: We report here an analysis of the MVMi virus structure and provide insights into tissue tropism, antigenicity and DNA packaging. Amino acids determining MVM tissue tropism were found to cluster on, or near, the viral surface. A conserved, glycine-rich, N-terminal peptide was seen to run through a cylindrical channel along each fivefold axis and may have implications for antigenicity. Density within the virion was interpreted as 29 ssDNA nucleotides per icosahedral asymmetric unit, and accounts for over one-third of the viral genome.

Conclusions: The presence of the glycine-rich sequence in the fivefold channels of MVMi provides a possible mechanism to explain how the unique N-terminal region of VP1 becomes externalized in infectious parvovirions. Residues that determine tropism may form an attachment recognition site for a secondary host-cell factor that modulates tissue specificity. The ordering of nucleotides in a similar region of the interior surface in the CPV and MVMi capsids suggests the existence of a genomic DNA-recognition site within the parvoviral capsid.

Addresses: [1]Department of Biological Sciences, Purdue University, West Lafayette, IN 47907-1392, USA and [2]Departments of Genetics and Laboratory Medicine, Yale University Medical School, New Haven, CT 06570, USA.

Present addresses: [†]Department of Biological Sciences, University of Warwick, Coventry CV4 7AL, UK, [‡]Departamento de Cristalografia, Instituto de Quimica-Fisica 'Rocasolano', CSIC, Serrano 119, 28006 Madrid, Spain and [§]Department of Infectious Diseases, Bethune University of Medical Sciences, 130021 Changchun, People's Republic of China.

*Corresponding author.
E-mail: mgr@indiana.bio.purdue.edu

Key words: genomic DNA structure, hemagglutination, murine parvovirus, tissue tropism, X-ray crystallography

Received: **29 June 1998**
Revisions requested: **10 August 1998**
Revisions received: **17 August 1998**
Accepted: **25 August 1998**

Structure 15 November 1998, **6**:1369–1381
http://biomednet.com/elecref/0969212600601369

Introduction

Minute virus of mice (MVM) is a member of the parvovirus family of small animal viruses which package their 5.5 kilobase single-stranded (ss) DNA genome within non-enveloped, $T = 1$ [1] icosahedral capsids. Parvoviral particles have an approximate maximum external radius of 140 Å and a molecular weight of ~4.2×10^6. Particles of MVM contain a total of 60 individual polypeptide chains that fall into three size classes, designated VP1, VP2 and VP3. There are about nine VP1 subunits per particle, the balance being made up of VP2 subunits in capsids lacking DNA (empty capsids) or a mixture of VP2 and VP3 subunits in full virions [2]. The dominant capsid protein, VP2, is the C-terminal 64 kDa region of the 83 kDa VP1 polypeptide. In DNA-containing particles, many VP2 proteins undergo cleavage during entry into the host cell, which removes approximately 20 residues from their N termini, to generate VP3 proteins [3–5]. This cleavage can be mimicked *in vitro* using trypsin, although peptide mapping indicates that the *in vitro* tryptic cleavage site may not be the natural cleavage site in MVM [4]. The N-terminal cleavage of VP2 only occurs in full particles, suggesting that the introduction of DNA into the particle allows the N terminus of VP2 to be externalized. Although the same amino acid sequence that is cleaved in VP2 is also present in VP1, the latter polypeptide does not appear to be cleaved at this position in either type of particle, *in vivo* or *in vitro*.

The three-dimensional structures of full and empty particles of canine parvovirus (CPV) [6–8] and empty particles of feline panleukopenia virus (FPV) [9], which like MVM are members of the same genus of autonomously replicating parvoviruses, have been determined to atomic resolution using X-ray crystallography. The 60 subunits of the parvoviral capsids contain the same eight-stranded (designated with letters B to I), antiparallel, β-barrel motif found in most other viral capsid structures [10]. The β barrel forms much of the contiguous shell of the capsid, although it makes up only one-third of the amino acid content of the capsid proteins. The remaining two-thirds of the

Table 1

VP2 amino acid differences between MVMi and MVMp.

	Amino acid sequence number*													
	10	160	232	317	321	362	366	368	388	402	410	440	455	551
MVMi	Gly	Ser	Ile	Ala	Glu	Val	Met	Arg	Ala	Asn	Arg	Asp	Thr	Val
MVMp	Ser	Leu	Val	Thr	Gly	Ile	Val	Lys	Ser	Ser	Lys	Asn	Ala	Ala
Position on MVMi structure†	N	S	B	B	S	B	S	S	S	B	S	S	B	B

*Residues are given in the three-letter amino acid code. †N, not ordered in structure; S, surface; B, buried.

capsid subunit structure is composed of very large insertions between the strands of the β barrel. The largest insertion loop consists of 217 amino acid residues between strands G and H, and forms part of the *22* Å long, 70 Å diameter spike protrusions present at the icosahedral threefold axes. An insertion between strands D and E forms an antiparallel β ribbon, which, together with similar insertions in four other fivefold-related polypeptides, forms a cylindrical structure about the icosahedral fivefold axes. Density observed within the channel created by these fivefold cylindrical structures, suggests that the N termini of some VP2 or VP1 molecules (one in five) can be externalized through this channel. This observation is consistent with the ability to cleave the N terminus of VP2 to form VP3 in assembled DNA-containing particles and with the externalization of the unique part of VP1, as shown by antibody precipitation. There is a 15 Å canyon-like depression circulating around each of the fivefold axes and a dimple-like depression at the twofold axes.

Host cell differentiation between viruses might occur at various stages of the viral life cycle, including cell-receptor attachment, viral entry, uncoating, DNA replication or transcription. Replication of autonomous parvoviruses is dependent upon cellular factors that are transiently expressed during the S phase of the cell cycle and also upon the differentiated state of the host cell [11–14]. Different strains of MVM show distinguishing pathological effects *in vivo* and have differing target cell specificity *in vitro* [11,14–17]. The prototype strain, MVMp, grows in fibroblasts, whereas the immunosuppressive strain, MVMi, productively infects erythroid progenitors [15] and T lymphocytes. The two allotropic strains, MVMp and MVMi, have been used as models for studying the molecular mechanism of parvoviral tropism. These viruses are 97% identical at the nucleotide level, differ by only 14 amino acids in their capsid proteins (Table 1) and are indistinguishable by neutralization with polyclonal antisera [18]. The restriction in tissue tropism between the two MVM strains is not due to a requirement for different cell-surface receptors because both strains of MVM virion compete for, and bind to, the same cell-surface receptor [14]. Hybrid cell lines, generated by the fusion of fibroblasts and T lymphocytes, are permissive for both strains of MVM, suggesting that the block in the restrictive cells is due to the lack of a differentiation-dependent cellular factor, which is virus strain specific [14,18]. The initial cell recognition appears to be followed by specific interactions with differentiation-dependent intracellular factors in the permissive host cell [19].

MVM tissue tropism has been shown to be primarily mediated by the viral capsid [18] and is, in part, determined by residues 317 and 321 in VP2 ('the allotropic determinants') [20,21], although a few copies of VP1 of either strain need to be present to obtain infection [*22*]. When these residues are alanine and glutamic acid, respectively, the virus exhibits lymphotropism; when these residues are threonine and glycine, the virus is fibrotropic [20]. If either one of the residues are altered an extended host-range mutant may result, allowing the virus to grow in both fibroblasts and T lymphocytes (Table *2*) [23,24]. The site-directed single mutants of MVMi, Ala317→Thr and Glu321→Gly, which carry only one of the two changes required for altering the MVMi lymphotropic strain to fibrotropic, are unable to grow in fibroblasts. Nevertheless, these mutants allow for the spontaneous selection of forward fibrotropic mutants, each of which contains an additional single amino acid change in VP2 (Table *2*) (F Wang, J Bratton and PT, unpublished results). The forward mutation is not always at one of the two original sites — 317 or 321.

Table 2

Forward mutants of the lymphotropic MVMi strain with a fibrotropic phenotype.

Site-directed mutation	Ala317→Thr	Ala317→Thr	Ala317→Thr	Glu321→Gly	Glu321→Gly	Glu321→Gly
Selected forward mutation*	Asp339→Gly	Asp399→Ala	Asp553→Asn	Ala317→Thr	Ser460→Ala	Tyr558→His

*These mutants were selected using the MVMi strain with single site-directed mutations.

Figure 1

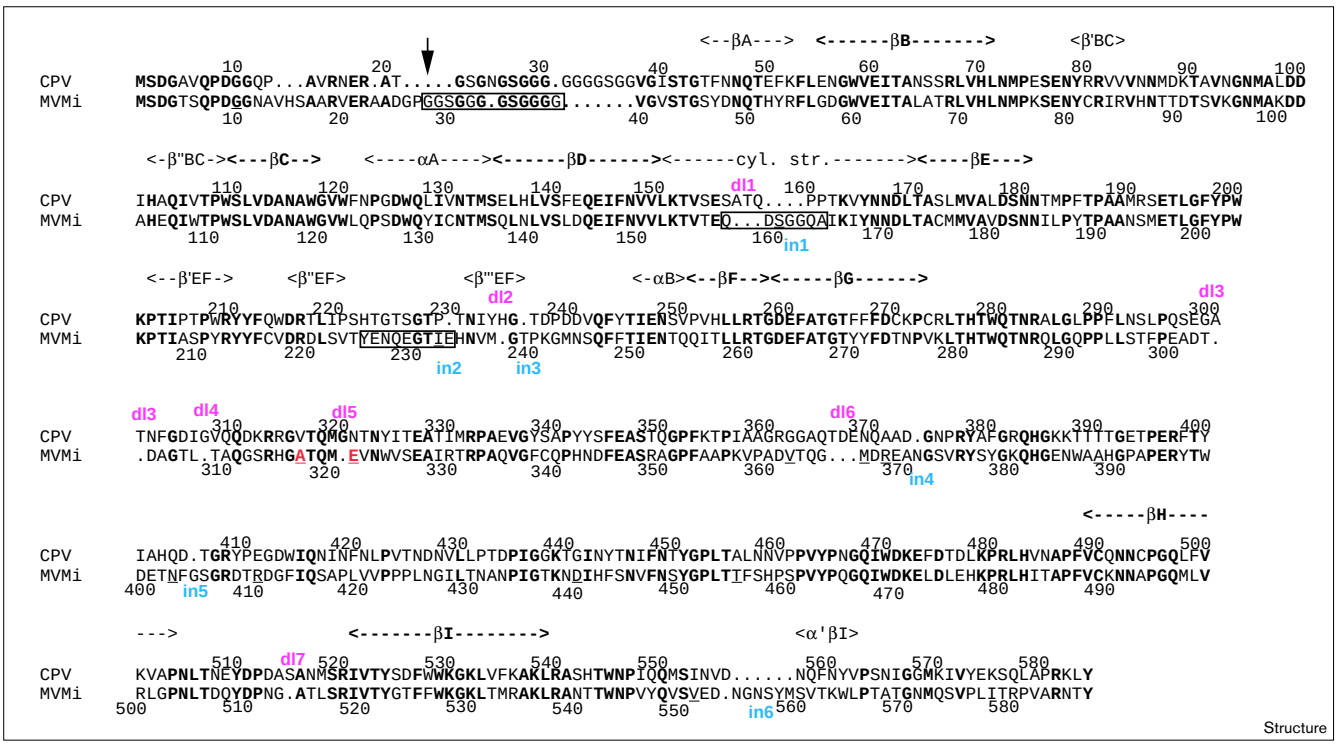

The amino acid sequence of MVMi. The alignment was made on the basis of a structural superposition of the VP2 capsid protein of CPV with that of MVMi. Secondary structure elements are labeled; residues that are conserved between CPV and MVMi are in bold and residues that differ between MVMi and MVMp are underlined. Regions of the amino acid sequence with insertions (in1–6, cyan) and deletions (dl1–7, magenta) in MVMi relative to CPV are indicated. The two allotropic residues of MVMi, 317 and 321, are shown in red. Less ordered regions in the MVMi electron-density map are shown boxed. The arrow indicates the first modeled residue.

The mechanism underlying the species specificity of CPV and FPV (which differ by only eight to ten amino acid residues in their capsid proteins) appears to be similar to that responsible for the tissue tropism differences observed for the two MVM strains. Both CPV and FPV bind to, and compete for, the same cell-surface receptor [25], but whereas CPV is able to replicate in canine and feline cells, FPV can only replicate in feline cell lines [26]. Canine cells transfected with FPV DNA, thus bypassing cell recognition and uncoating, can produce virus, suggesting that host-range selection is likely to occur at an early stage of infection [25]. The residues determining host range [27,28] are clustered on the capsid surface, located either on the shoulder of the icosahedral threefold spikes or around the edges of the twofold dimple-like depression [9]. Thus, the twofold dimple has been postulated as a possible site of interaction with cellular factors that determine host range and tissue tropism.

Regions of partially ordered nucleic acid have been reported for a number of viruses. DNA-containing particles of CPV have at least 11 icosahedrally ordered DNA bases [6]. In CPV, the nucleotide bases form the majority of contacts with the capsid protein and were interpreted to have a slight preference for specific nucleotides in some of the individual binding sites [29]. This sequence specificity of DNA–protein interaction was suggested to be the basis of viral genome recognition during encapsidation [29]. Icosahedrally ordered ssDNA was also observed in the interior of the bacteriophage ϕX174 capsid [30]. Icosahedrally ordered RNA has been found in bean pod mottle virus [31], flock house virus [32], nodamura virus [33], various plant satellite viruses (reviewed in [34]), and to a lesser extent in human rhinovirus 16 (HRV16) [35], HRV14 [36], coxsackievirus B3 [37] and poliovirus 3 Sabin [38]. In the RNA viruses, nonspecific interactions were observed between the sugar–phosphate backbone and the protein. In contrast, parts of the RNA genome of the bacteriophage MS2 bind to the capsid protein involving extensive contacts with nucleotide bases [39].

We report here the functional implications of the atomic structure of full virions of MVMi, particularly with respect to tissue tropism and with reference to the encapsidated genomic DNA. A comparison is made between the MVMi structure and those of other parvoviruses.

Details of the structure determination procedure were reported earlier [40].

Results and discussion

Protein structure and comparison with other parvoviruses

The MVMi polypeptide was modeled into a 3.5 Å resolution map, computed with F_{obs} amplitudes and phases derived from the icosahedrally averaged density, using the program O [41]. All residues were built from amino acid 28 to the last C-terminal residue 587, including some regions of weaker density (Figure 1). Although the MVMi amino acid sequence is only 50% identical to that of CPV (Figure 1) and FPV [42], the structures of MVMi, CPV and FPV are mostly similar except for certain surface loops. The structure and position of the β barrel within the icosahedral asymmetric unit (Figure 2) are conserved among the three viruses. The channel at the fivefold icosahedral axis, surrounded by the fivefold cylindrical structure, is also conserved in MVMi. The surface features of the MVMi capsid, like those of CPV and FPV [6,9], include protrusions at the icosahedral threefold axes, dimple-like depressions at the icosahedral twofold axes and canyon-like regions around the fivefold axes (Figure 3).

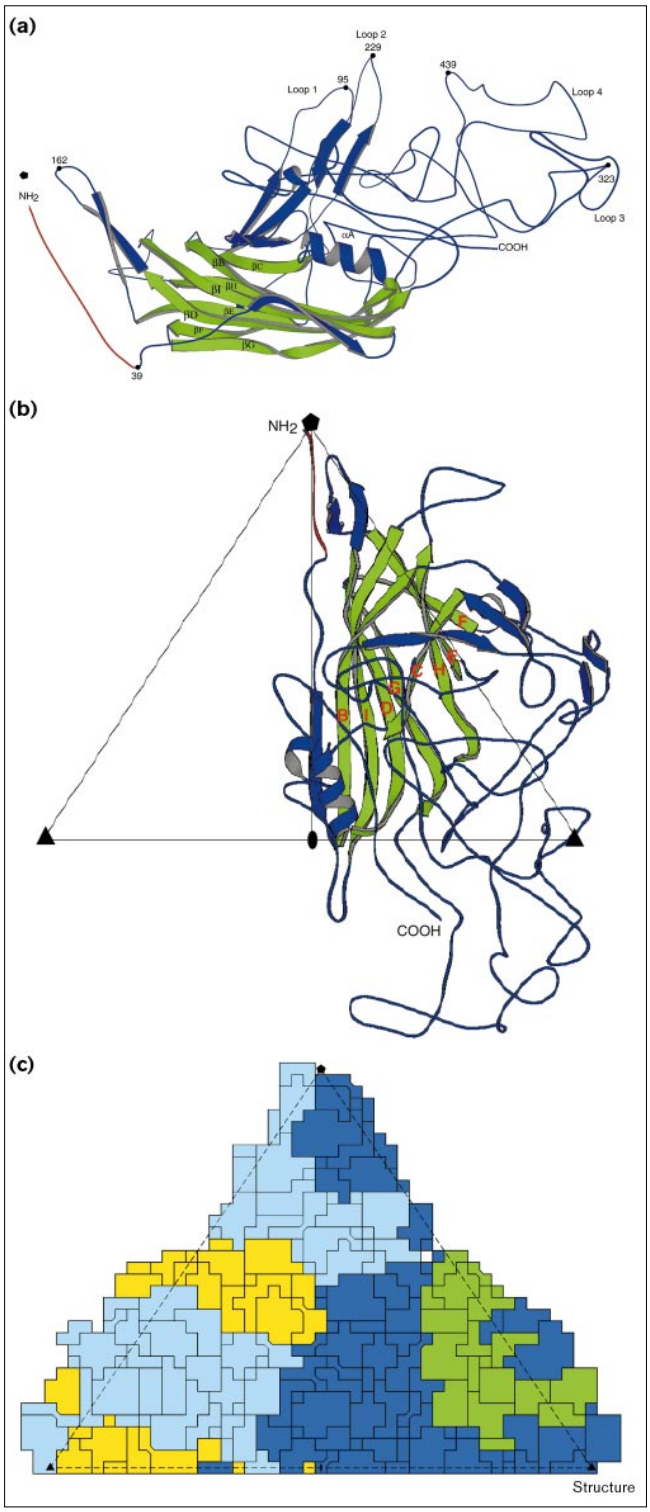

The largest differences in Cα positions between MVM and CPV occur on the capsid surface around the icosahedral threefold axes and the regions surrounding the depressions at the icosahedral twofold and fivefold axes. The majority of the differences are associated with regions of amino acid insertions (six in total) and deletions (seven in total) in MVMi relative to CPV (Figure 1).

The first insertion in the MVMi sequence (residues 159–162) relative to CPV occurs in the β ribbons around the fivefold axes (Figure 1), causing a change in topology which constricts the top of the cylindrical structures in MVMi relative to CPV (Figure 4a). The second insertion, residue 233, occurs in loop 2 which forms part of the top of the threefold protrusions, partially contributing to an ~4 Å extension of the threefold protrusion in MVMi compared to that of CPV. Two other insertions (third and fifth, at residues 239 and 404, respectively) are in the

Figure 2

The MVMi VP2 capsid protein. **(a)** The topology of VP2 showing the location of the strands making up the eight-stranded β barrel (green), the fivefold β ribbon and the location of the four major surface loops 1 to 4. The N-terminal glycine-rich sequence located within the fivefold channel is shown in red; the rest of the molecule is in blue. Some amino acid sequence numbers are also shown. **(b)** The location of one VP2 subunit within a geometrically defined asymmetric unit viewed down an icosahedral twofold axis. The fivefold axis is represented as a black pentagon, the threefold axes as triangles and the twofold axis as an oval. The color scheme is the same as in (a). **(c)** A two-dimensional 'roadmap' of MVMi, showing the contribution of VP2 subunits in one icosahedral asymmetric unit. Dark blue represents the reference subunit as shown in (b). Yellow represents a subunit related by a twofold rotation about the axis shown in the center of the base of the triangle. Green represents a subunit related by a threefold rotation about the threefold axis at the bottom right of the triangle. Cyan represents a subunit related by a rotation about the fivefold axis at the top of the triangle. The projection is down a twofold axis. (Figures (a) and (b) were drawn with the program MOLSCRIPT [57], (c) was drawn with the program roadmap [58].)

dimple region. These two insertions are adjacent to the sixth insertion (residues 553–559), the largest in MVMi relative to CPV, resulting in a five amino acid addition (Figure 4b) in the dimple-like depression at the icosahedral twofold axes. This sixth insertion causes a small protrusion within the MVMi dimple. The fourth insertion in the MVMi sequence (residue 371, not visible on a surface projection down the twofold axis) is part of a loop with a variable conformation between CPV and FPV, termed the 'hemagglutination' loop [9] (see below). This insertion is in a region associated with the largest structural differences between FPV and CPV.

The seven deletions in MVMi relative to CPV all occur on the viral surface. Two of the deletions (residues 320 and 366–368 of CPV, dl5 and dl6 in Figure 1) are close to the allotropic determinants (residues 317 and 321 of MVMi; Figure 4c) and the hemagglutination loop, located on the wall of the icosahedral twofold dimple-like depression. The deletion of CPV residues 300, 301 and 307 (dl3 and dl4 in Figure 1) removes a hydrophobic patch that forms part of an antigenic site and a host range determining region in CPV [41,42] (Figure 4d). The deletions at residues 300, 301, 307 and 515 result in surface differences on the wall surrounding the canyon-like depression.

The conformational differences between MVMi and CPV in the vicinity of residues 388–391 can be attributed to the different properties of Glu384 in MVMi compared to the equivalent residue (Lys386) in CPV. Structural sensitivity to changes of amino acids in this region have previously been described for the host-range and antigenic mutant of CPV, Ala300→Asp [43], and are also observed between CPV and FPV.

The icosahedral threefold spike extension in MVMi is caused partially by a difference in amino acid type at position 95 in MVMi (equivalent to position 93 in CPV) at the top of loop 1 and partly due to the second insertion (residue 233) as mentioned above. The sidechain Asn93 in loop 1 of CPV points towards the interior of the virus, whereas in MVMi this residue is a lysine, which points outwards and towards loop 2 where its amino group hydrogen bonds with the carbonyl oxygen of residue 230. The region of the capsid containing residue 93 of CPV and the top of loop 2 form part of a dominant antigenic epitope in CPV and FPV. Residue 93 is also involved in CPV host-range determination. A mutation of residue 93 from asparagine in CPV to lysine in FPV causes a major conformational change in this antigenic region [9]. The Asn93→Lys mutation in CPV results in the inability of a number of CPV-specific monoclonal antibodies to neutralize its infectivity [44] and abolishes the ability of the virus to grow in canine cells *in vitro* [27].

Figure 3

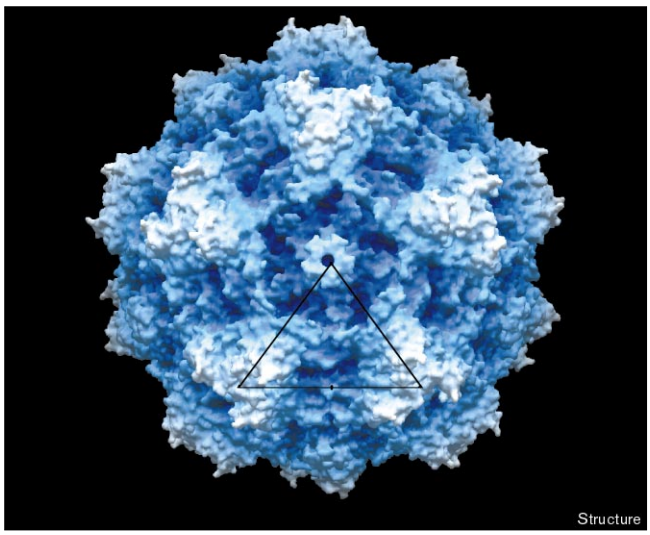

The MVMi capsid. Depth-cued representation of a whole MVMi particle. The particle surface shading is based on distance from the viral center: the lighter regions represent residues that are at the greatest radial distance and the darkest regions represent residues at the shortest radial distance. The icosahedral fivefold, threefold and twofold axes for one viral asymmetric unit are indicated.

The N-terminal glycine-rich region and possible mechanisms for surface exposure

As observed for CPV and FPV [6,9], there is density (height of 2.0σ) extending along the fivefold channels of the MVMi capsid. This was modeled as the glycine-rich N-terminal region (residues Gly28-Gly-Ser-Gly-Gly-Gly-Gly-Ser-Gly-Gly-Gly38) of VP2 (Figures 1 and 5a) [7,8], a sequence that is highly conserved among animal and insect parvoviruses [42]. Residue 39 is the first N-terminal residue that is differentiated from its fivefold symmetry-related neighbors. Density (height of 1.5σ) extending into the interior of the capsid was modeled as N-terminal residues Gly36-Gly-Gly38, representing the other non-externalized VP2 subunits (Figure 5b). This is consistent with biochemical data showing that the N termini of only some VP2 subunits are externalized for cleavage to VP3 in virions [3,4]. Presumably, one in five of the VP2 N termini is externalized and is available for cleavage, while the other four N-terminal ends are within the capsid. The suggestion that the fivefold channel is the site of externalization of the N-terminal peptide during maturation cleavage of the genus *Parvovirus* is further supported by the observation that the fivefold channel appears closed in low resolution cryoelectron microscopy studies of human parvovirus B19 [45,46] and Aleutian mink disease parvovirus (R McKenna, *et al.*, and MA-M, unpublished results), where the VP2 to VP3 virion maturation cleavage does not occur.

The MVMi N-terminal peptide running through the fivefold channel contains only glycine residues, except for

Figure 4

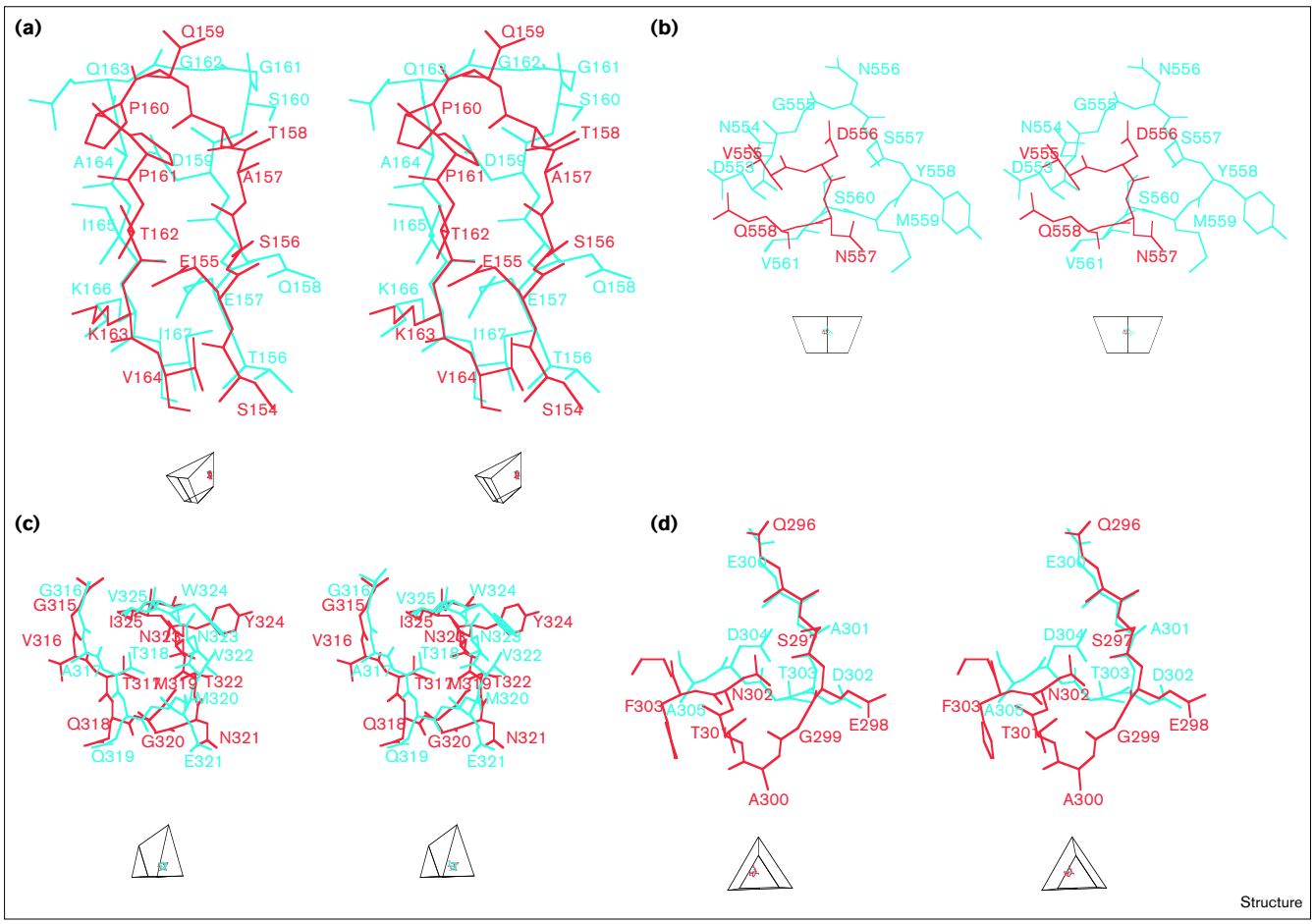

Stereoviews illustrating the mainchain differences between MVMi (blue) and CPV (red). **(a)** Differences in the residues lining the fivefold channel. **(b)** The six-residue insertion (MVM residues 554–559). **(c)** Differences in the 'allotropic' region (MVM residues 315–326 are shown). **(d)** The antigenic region near CPV residue 300, where there is a three-residue deletion in MVMi relative to CPV. The orientation and position of the subunits are represented by a minidiagram showing the icosahedral asymmetric unit in the same orientation. The orientation of (c) and (d) is looking down the twofold axis. (Figures were generated using the program MacInPlot [59].)

serines 30 and 35. The sidechain of Ser35 is indicated by the shape of the density within the channel. The constriction at the top of the MVMi channel relative to CPV (Figure 4a) is consistent with the presence of glycines in the N-terminal extension of MVMi. *In vitro*, trypsin digestion of full virions of most members of the genus *Parvovirus* occurs at two sites, resulting in two small peptides and the VP3 polypeptide which still contains the glycine-rich sequence [47]. As the two arginine residues (Arg19 and Arg22 in MVMi, and Arg16 and Arg19 in CPV) are the *in vitro* tryptic sites, then the current models for MVMi and CPV are consistent with the immediate accessibility of these sites for one in five VP2 molecules at the exterior surface of the virion. The finding that most VP2 molecules can be cleaved in this way suggests that a dynamic situation exists at the fivefold channel. In one model, the newly created N terminus of a VP3 molecule could withdraw into the virion after cleavage and be replaced at the surface by an uncleaved VP2 N terminus. This would be cleaved in turn, until most of the VP2 N termini, initially sequestered within the virion, are converted to VP3.

VP2 cleavage occurs *in vivo* during host cell entry. This process may be required for virion translocation across the plasma membrane [47]. The externalization of the N termini of VP2 may be analogous to the externalization of the minor capsid protein, VP4, of picornaviruses after virus attachment and during uncoating, which has also been suggested to occur through the fivefold β cylinder [48]. Immunoprecipitation studies of MVMi have shown that, after limited heating, full virions, but not empty capsids, can be precipitated using antibodies raised against peptides from the VP1 unique region. This region is normally sequestered within the virion, but becomes exposed

Figure 5

Stereoviews of the fivefold channel with modeled N-terminal peptides. The glycine-rich sequence in MVMi is shown in ball-and-stick representation, colored according to atom type; CPV is shown in red stick representation. The surrounding fivefold channel for MVMi is in blue and green corresponding to two fivefold-related subunits. **(a)** Externalization of the N-terminal extension towards the top of the figure. **(b)** Internalization of the N-terminal extension. (The figure was drawn with the program MacInPlot [59].)

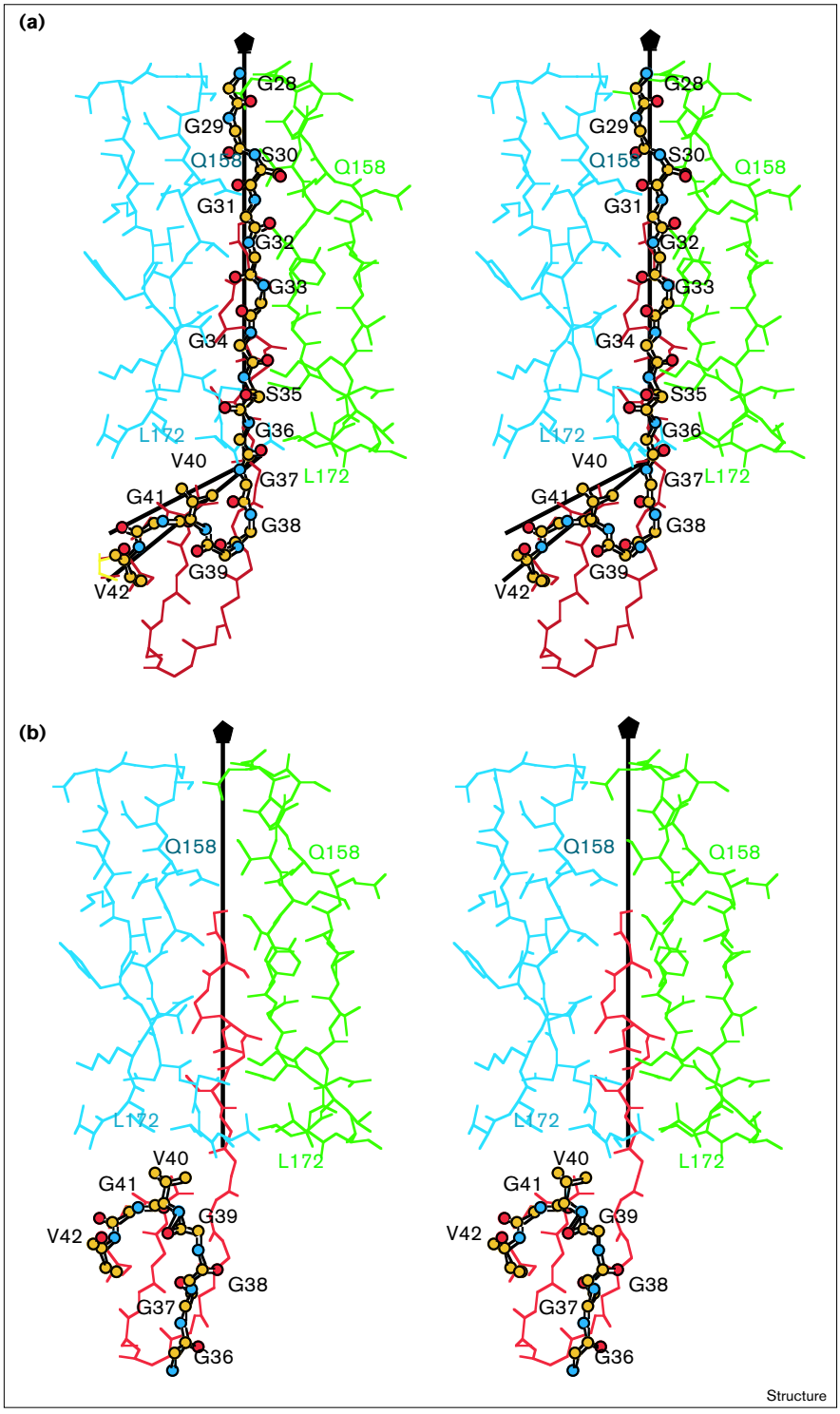

on heating without substantial rearrangement of the rest of the viral shell [49]. This dynamic flexibility is also consistent with that found in the externalization of VP4 and the N-terminal end of VP1 in the picornaviruses [50,51] and the insect flock house virus [52].

Hemagglutination dependence on pH

CPV is able to hemagglutinate Rhesus monkey erythrocytes under all conditions of pH, whereas FPV hemagglutinates only when the pH is less than 6.2. The largest structural differences between CPV and FPV [9], both

Figure 6

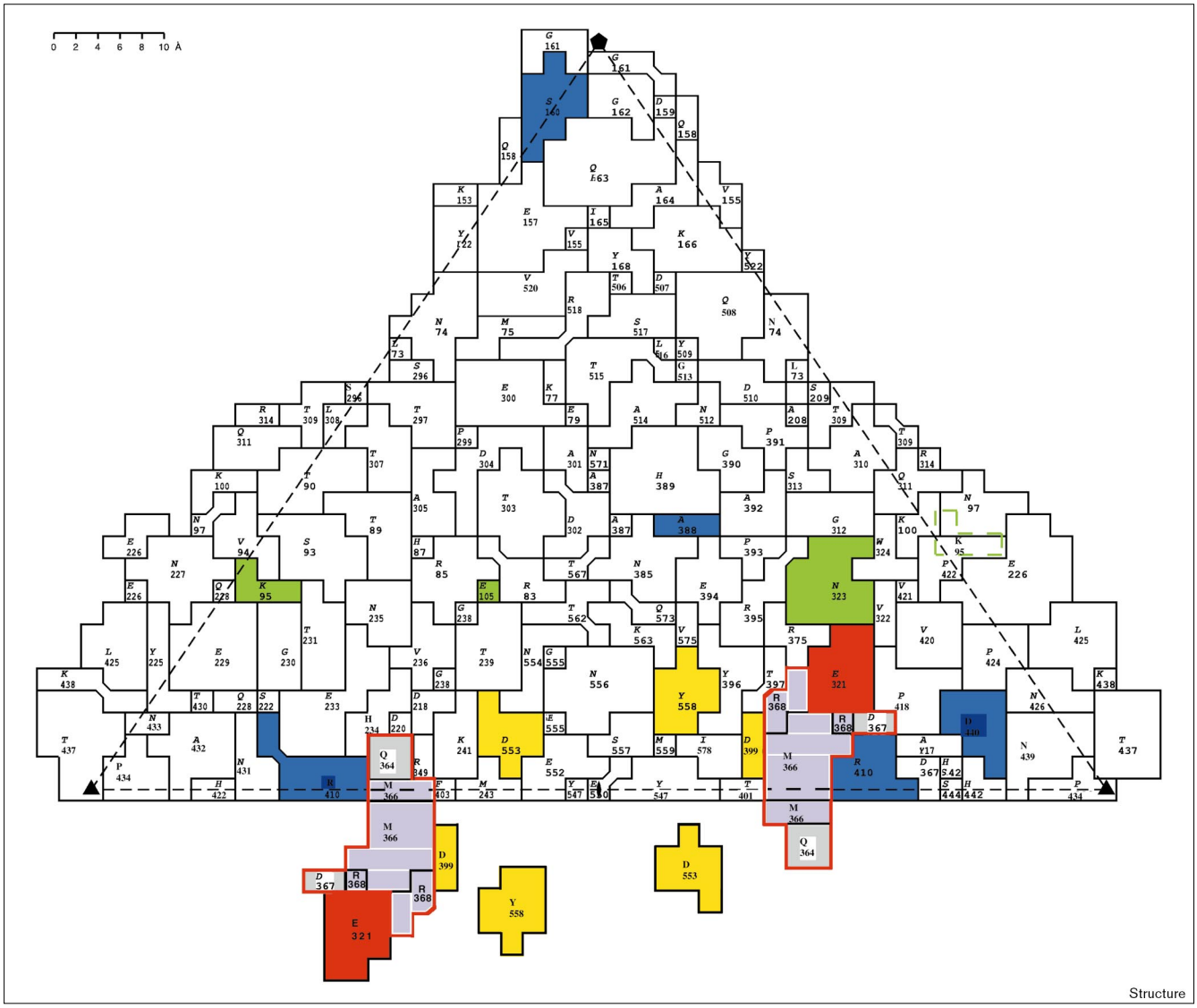

Roadmap of MVMi showing capsid surface residue functions. The residues are color coded: red outline, residues in the hemagglutination loop; purple, residues in the hemagglutination loop that differ between MVMi and MVMp; gray, residues in the hemagglutination loop that are the same in MVMi and MVMp; red, MVM residues that participate in the determination of tissue tropism; yellow, MVM forward mutations (see text and Table 2 for details); blue, residues that are different in MVMi and MVMp, but do not participate in tissue tropism; green, CPV residues that determine host range (shown are MVM equivalent residues); green outline, position of MVMi residue 95 (equivalent to CPV residue 93) in the reference subunit shown in Figure 2. Some of the residues near the twofold axis are also shown in their symmetry-related positions. (The figure was drawn with the program roadmap [58].)

determined at pH 7.5, occur in a surface loop between residues 356 and 374, although there are no amino acid differences in this loop. Not only does the loop have completely different conformations in these two viruses, but in CPV the loop is more disordered than in FPV. Mutational analysis (Table 3) [27,53] has shown that the hemagglutination behavior is determined by residues 323, 375 and 377, all of which are positioned adjacent to the hemagglutination loop. It has, therefore, been assumed that the CPV structure of the loop represents a conformation able to bind erythrocytes, whereas the FPV structure would be a non-hemagglutinating structure. These conclusions were questioned in a study of the structure of the CPV mutant Ala300→Asp [43] in which the loop is FPV-like, but the hemagglutination properties are CPV-like.

MVMi hemagglutinates erythrocytes under physiological conditions, and in this respect is like CPV. However, the

Table 3

Hemagglutination properties of CPV-like parvoviruses.

	Residue*			pH-independent CPV-like	pH-dependent FPV-like	Non-hemagglutinating
	323	375	377			
CPV-d†	Asn	Asn	Arg	✓		
CPV2 (Ala300→Asp)	Asn	Asn	Arg	✓		
CPV2 (Arg377→Lys)	Asn	Asn	Lys			✓
FPV-b	Asp	Asp	Arg		✓	
MVMi	Asn	Ser	Arg	✓		

*Residues are given in the three-letter amino acid code. †These viruses correspond to those described in [27] and [55].

hemagglutination behavior of MVMi has not been investigated over a wide range of pH. The hemagglutination loop in MVMi is fairly well ordered and has a structure closer to, but not the same as, FPV than to CPV. Inspection of Table 3 suggests that FPV-like behavior might be brought about by the charge on the carboxy groups of CPV residues 323 and 375, causing conformational changes in the surface hemagglutination loop. These conformational changes presumably determine the ability of the virus to interact with erythrocytes.

Tissue tropism

Seven of the 14 amino acids that differ between MVMi and MVMp (Table 1), including the allotropic residue 321, occur on the capsid surface (Figure 6), while the remaining seven, as well as the allotropic residue 317, are immediately underneath the capsid surface. Of the differing residues, 12 cluster around the edge of the icosahedral threefold spike or are in the twofold dimple-like depression (Figure 6). Three of the five selected 'forward' amino acid mutations (residues 399, 553 and 558; Table 2), which confer fibrotropism to single site-directed MVMi mutants, also occur on the surface and are located in the twofold dimple-like depression (Figure 6).

Thus, the residues that confer fibrotropism are on or near the surface of the particle, at the base of the threefold spike or in the twofold dimple-like depression (Figure 6). This implies that the allotropic determinant is probably a surface feature on the assembled virion, possibly representing the binding site for a putative intracellular 'receptor'. The region on the capsid surface in which the MVM tissue tropic determinants are clustered overlaps with the positions of the amino acids that differentiate host-cell specificity for CPV and FPV [9].

Residues that participate in altering tissue tropism from the lymphotropic MVMi strain to the fibrotropic MVMp strain appear to create instability in the structure (Table 4; Figure 7). The allotropic mutant Ala317→Thr would create a steric clash with Thr331, and the allotropic mutant Glu321→Gly removes the counter charge to Arg368 on the viral surface. Similarly, the selected fibrotropic mutants Asp399→Gly or Asp399→Ala also remove a counter charge to Arg368. The selected fibrotropic mutant Ser460→Ala removes a hydrogen bond to the surface residue Glu400. These broken or strained interactions are across the boundary between adjacent subunits in the capsid. Finally, the mutants Asp553→Asn and Tyr558→His alter the surface charge within the area likely to be the site of interaction with a cellular factor. While these changes are predicted to confer some instability on the fibrotropic virion, compared with that of MVMi, the fibrotropic coat might rather adopt a subtly alternative structure in this region. This altered structure would allow the virion to engage a different intracellular receptor, expressed in fibroblasts rather than lymphocytes, that is required to facilitate a crucial step early in the viral life cycle. This possibility awaits solution of the structure of a fibrotropic host range switch mutant and its comparison with the present structure of the lymphotropic virus.

Table 4

Instability in the fibrotropic MVMp structure as deduced by model building.

Residue	Lymphotropic MVMi structure*	Fibrotropic MVM model*	Comments on fibrotropic model
317	Ala	Thr	Steric clash with Thr331
321	Glu	Gly	Leaves Arg368 without charge cancellation
399	Asp	Gly	Leaves Arg368 without charge cancellation
399	Asp	Ala	Leaves Arg368 without charge cancellation
460	Ser	Ala	Eliminates hydrogen bond with Glu400
553	Asp	Asp	Alters surface charge
558	Tyr	His	Alters surface charge

*Residues are given in the three-letter amino acid code.

Figure 7

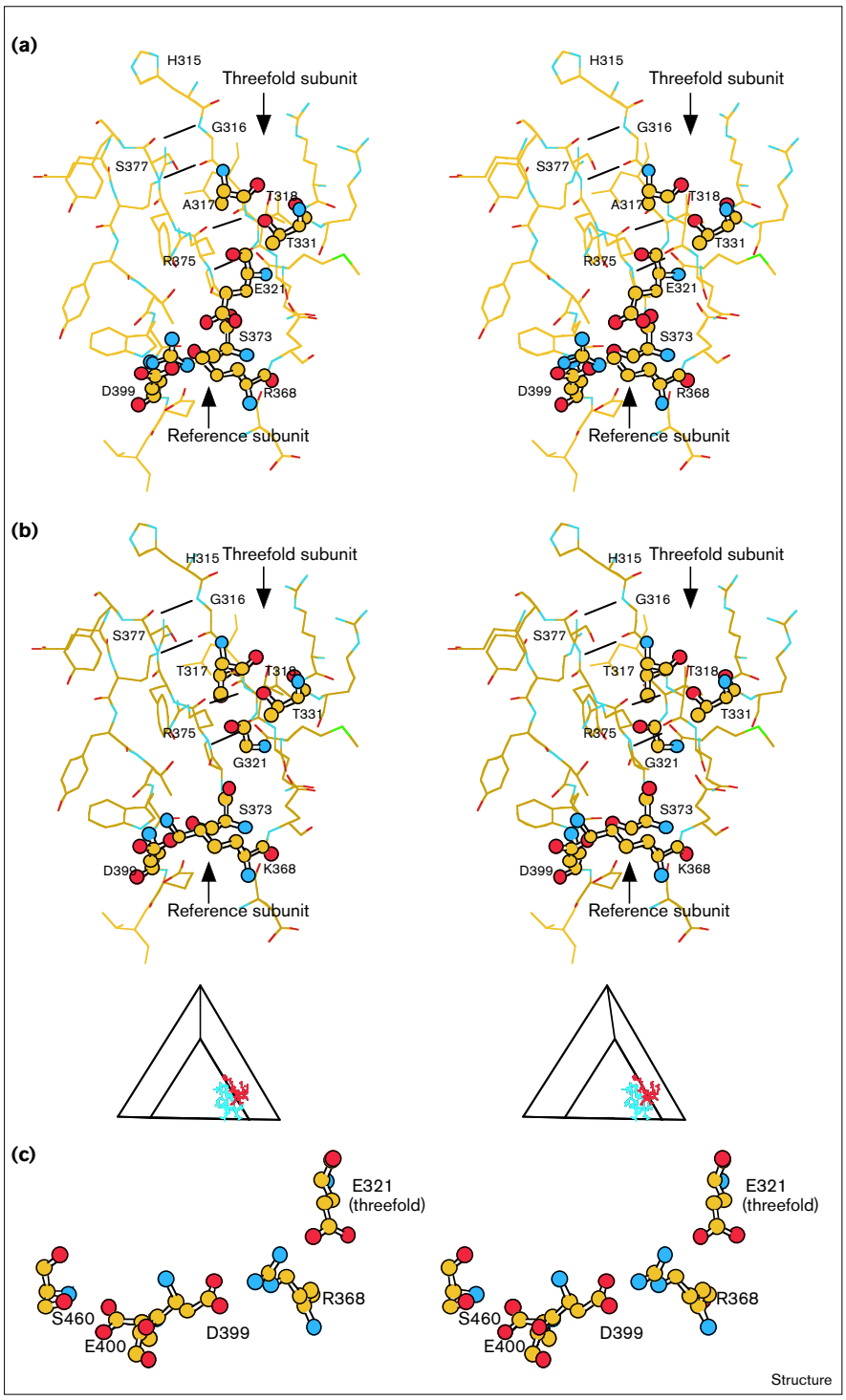

Stereoviews showing interactions of the allotropic residues 317 and 321. The residues as observed in **(a)** the MVMi capsid and **(b)** modeled for the MVMp capsid. Atoms are colored according to type: carbon, yellow; nitrogen, blue; and oxygen, red. The orientation and position are shown with respect to the icosahedral triangle. **(c)** The chain of interactions that are disrupted in selected forward fibrotropic mutations (see Table 4). (The figures were drawn with the program MacInPlot [59].)

DNA structure

A difference map between full and empty CPV particles showed a substantial amount of electron density in the interior of the particles [6]. This density was interpreted in terms of 11 DNA nucleotides per icosahedral asymmetric unit chelated by two metal ions. Wu and Rossmann [54] had shown that the structured DNA causes small, but significant, conformational changes to the inside surface of the CPV capsid, representing a nonspecific DNA–protein binding site. A difference map between full and empty

Figure 8

Stereoview showing the ordered ssDNA density within the MVMi virion. The red structure is common to MVMi and CPV. The blue structure is present in MVMi and may also be present, albeit not as well ordered, in CPV. The position and orientation of the structure within the icosahedral asymmetric unit is also shown. (The figure was drawn with the program MacInPlot [59].)

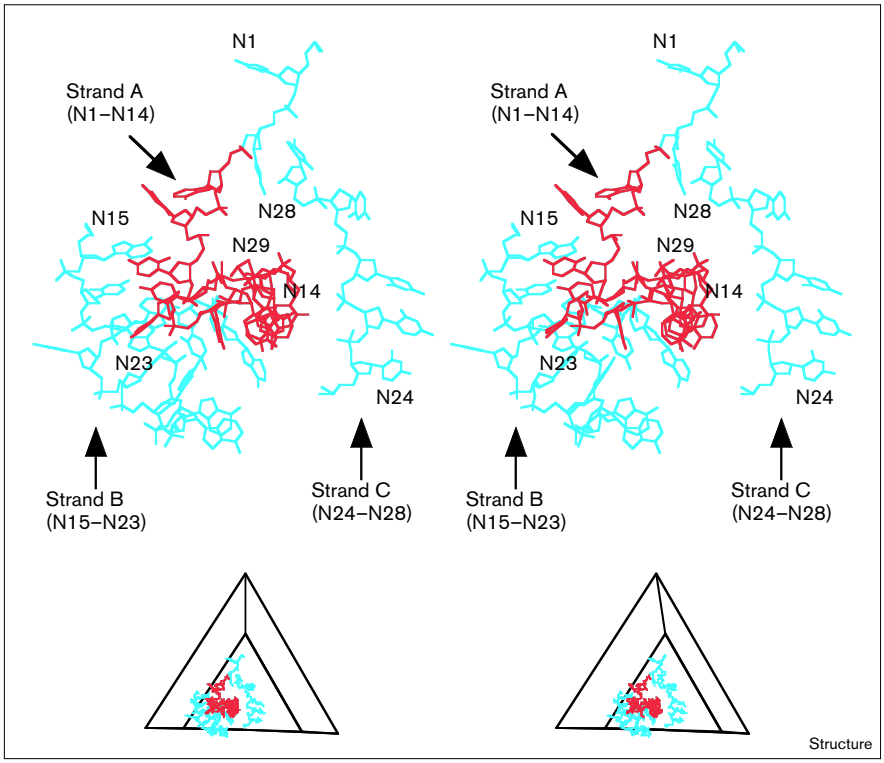

MVMi particles showed substantially more density than was interpretable for CPV [40]. The electron-density map for the full MVMi particles was used to interpret the DNA structure. In this map, the average protein density and also the icosahedrally 'well ordered' 23 DNA bases (Figure 8) had a height of 3σ, and six 'less ordered' DNA bases had a height of around 1.5σ.

Two nucleic acid strands, A (nucleotides N1–N14) and B (N15–N23), were built into well-ordered density, while another strand, C (N24–N28), and one unconnected nucleotide, N29, were built into less ordered density (Figure 8). These 29 bases, taken together with the icosahedral symmetry-related bases, amount to 34% of the total genome. The ten contiguous nucleotides (N3–N12) in strand A, and the two chelating metal ions, occur at equivalent positions to those observed in the CPV structure [29]. All of the additional 17 nucleotides built into the MVMi density correspond mostly to weaker density that was not interpretable for CPV.

In the MVMi particles, the chain direction of nucleotides in strands A, B and C was evident from the relative position of the sugars, phosphates and bases. The sugar–phosphate backbone of strand A, stabilized by two metal ions, is associated with a cavity in the interior of the capsid [8,29]. The 5′ ends of strands A and C are close to the fivefold axes. Strand B has an extended backbone and forms both sugar–phosphate interactions, as well as base interactions with the surrounding protein. All the DNA strands are stabilized by extensive interbase and intrabase stacking interactions (Figure 8). There are five distinct stacks: (N5, N11, N17, N23); (N6, N19, N20); (N8, N9, N10, N12, N13, N14); (N15, N16); and (N21, N22). In addition, N2 of strand A stacks with N28 from strand C. The 3′ end of strand C is close to the icosahedral twofold axes where its bases continue the stack with twofold symmetry-related bases.

Analysis of the CPV structure [29] had shown that some specificity was associated with the interaction between the DNA bases and the capsid protein. The sequence of bases corresponded to a low degree of repetition within the DNA genome, suggesting that there was some specificity in the DNA-binding site on the internal, icosahedrally repeated, surface of the viral capsid. Most of the CPV residues involved in binding DNA bases are conserved in MVM. However, no analysis has been made of the MVM DNA sequence to determine whether the same pattern of bases occurs in MVM as in CPV. Nevertheless, in light of the conservation of the base-binding sites, it is probable that the same specific DNA-recognition site is conserved between these viruses.

Biological implications

Parvoviruses are small, 280 Å diameter, single-stranded DNA-containing icosahedral viruses with a capsid that

contains 60 subunits of three types — VP1, VP2 and VP3. The capsid contains only a few subunits of type VP1; most of the capsid comprises VP2 subunits. VP1 and VP2 have a common C-terminal domain of about 585 amino acids that constitute the viral coat. Some of the VP2 N termini are cleaved off at the stage of cell binding during maturation to generate VP3 subunits. This process may be necessary for viral translocation from the plasma membrane to the nucleus. The structure of the murine parvovirus, minute virus of mice (MVM), shows the highly conserved, N-terminal glycine-rich sequence of VP2 in the channel along the fivefold axes of the virion, as was also found in the structure of canine parvovirus (CPV). This provides further evidence that some of the N-terminal regions of VP2 in parvoviral virions must be externalized during the maturation cleavage.

Following initial host cell entry, the capsid structure of parvoviruses plays a major role in determining tissue tropism and host-range specificity. Residues determining the tissue specificity of the immunosuppressive, lymphotropic MVMi strain and the fibrotropic MVMp strain cluster on the viral surface. Residues within the cluster are derived from symmetry-related subunits, indicating that the tissue tropic determinants are a feature only on assembled virions. Model building suggests that MVMp adopts a locally different structure to that of MVMi, allowing these MVM strains to engage different intracellular receptors, expressed in fibroblasts and lymphocytes, respectively. This receptor recognition is required to facilitate a crucial step early in the viral life cycle. Residues that determine host-cell specificity between CPV and feline panleukopenia parvoviruses (FPV) are also found on the capsid surface in a region overlapping those that determine MVM tissue tropism. Hence, this region may be the binding site for host-cell factors, but not necessarily those factors involved in the initial recognition event as tissue and host-cell specificities appear to be modulated after viral entry. The same region also overlaps the surface 'hemagglutination loop' which is probably required for binding to an erythrocyte receptor.

Difference electron-density maps used to compare DNA-containing and empty MVMi particles show extensive ordered structure within the DNA-containing capsid. Much of this density was interpreted as 29 ordered, or partially ordered, deoxynucleotides per icosahedral asymmetric unit, arranged mostly in three separate strands in five stacks. Ten of these nucleotides have a similar structure in CPV. The icosahedral ordering of nucleotides, and conservation of base-binding sites between MVMi and CPV, identifies a DNA-recognition site on the parvoviral capsid interior.

Materials and methods

Protein structure

MVMi particles were propagated and purified using a modified procedure of Tattersall and Bratton [18]. Crystals were grown using the hanging-drop vapor diffusion method [55]. X-ray diffraction data were collected for the empty and full particle crystals at the F1 station of the Cornell High Energy Synchrotron Source (CHESS) [40]. The crystals were monoclinic, belonging to space group *C*2, with cell dimensions of $a = 448.7$ Å, $b = 416.7$ Å, $c = 305.3$ Å and $\beta = 95.8°$. The data set for DNA-filled MVMi particles contained 280 images from 35 crystals, representing 65% of all possible data to 3.5 Å resolution with an R_{merge} of 15.5%. The data for the empty particles were less complete, consisting only of 45 images from five crystals, representing 13% of data completeness with an R_{merge} of 15.1%. The data set for the full particles of MVMi was used in the structure determination. The homologous CPV structure was used as a phasing model to initiate the molecular replacement electron density averaging procedure. The program O [41] was used to build the model of MVMi.

DNA structure

The DNA density common to that observed in the CPV virion structure was modeled using the program O [41], starting with the CPV DNA coordinates [29] as an initial guide. C2′-*endo* and C3′-*endo* ribose conformations were used for the sugar puckers, and commonly occurring glycosidic angles [56] were used to obtain the best fit of the bases.

Accession numbers

The coordinates and structure factors for the MVMi virion structure have been deposited with the Brookhaven Protein Data Bank with accession codes 1MVM and R1MVMSF, respectively.

Acknowledgements

We are grateful to our many Purdue University colleagues who participated at CHESS in collection of the data used in the structure determination and to the helpful CHESS staff. We thank Cheryl Towell and Sharon Wilder for their help in the preparation of the manuscript and Jean-Yves Sgro at the University of Wisconsin for making Figure 3. The work was supported by National Institutes of Health grants to MGR (AI 11219) and to PT (CA 29303), a Markey Foundation grant to Purdue University, in part by a Research and Teaching Innovations Fund award from the University of Warwick, England to MA-M, a Spanish Ministry of Education Fellowship to ALL-S, and in part by a WHO/PAHO Postdoctoral Fellowship to FW.

References

1. Caspar, D.L.D. & Klug, A. (1962). Physical principles in the construction of regular viruses. *Cold Spring Harbor Symp. Quant. Biol.* **27**, 1-24.
2. Tattersall, P., Cawte, P.J., Shatkin, A.J. & Ward, D.C. (1976). Three structural polypeptides coded for by minute virus of mice, a parvovirus. *J. Virol.* **20**, 273-289.
3. Clinton, G.M. & Hayashi, M. (1976). The parvovirus MVM: a comparison of heavy and light particle infectivity and their density conversion *in vitro*. *Virology* **79**, 57-63.
4. Tattersall, P., Shatkin, A.J. & Ward, D.C. (1977). Sequence homology between the structural polypeptides of minute virus of mice. *J. Mol. Biol.* **111**, 375-394.
5. Paradiso, P.R. (1981). Infectious process of the parvovirus H-1: correlation of protein content, particle density, and viral infectivity. *J. Virol.* **39**, 800-807.
6. Tsao, J., *et al.*, & Parrish, C.R. (1991). The three-dimensional structure of canine parvovirus and its functional implications. *Science* **251**, 1456-1464.
7. Wu, H., Keller, W. & Rossmann, M.G. (1993). Determination and refinement of the canine parvovirus empty-capsid structure. *Acta Cryst. D* **49**, 572-579.
8. Xie, Q. & Chapman, M.S. (1996). Canine parvovirus capsid structure, analyzed at 2.9 Å resolution. *J. Mol. Biol.* **264**, 497-520.
9. Agbandje, M., McKenna, R., Rossmann, M.G., Strassheim, M.L. & Parrish, C.R. (1993). Structure determination of feline panleukopenia virus empty particles. *Proteins* **16**, 155-171.
10. Rossmann, M.G. & Johnson, J.E. (1989). Icosahedral RNA virus structure. *Annu. Rev. Biochem.* **58**, 533-573.
11. Siegel, G. (1984). Biology and pathogenicity of autonomous parvoviruses. In *The Parvoviruses.* (Berns, K.I., ed.), pp. 297-362, Plenum Publishing Corporation, New York, NY.

12. Miller, R.A., Ward, D.C. & Ruddle, F.H. (1977). Embryonal carcinoma cells (and their somatic cell hybrids) are resistant to infection by the murine parvovirus MVM, which does infect other teratocarinoma derived cell lines. *J. Cell Physiol.* **91**, 393-402.
13. Tattersall, P. (1978). Susceptibility to minute virus of mice as a function of host-cell differentiation. In *Replication of Mammalian Parvoviruses.* (Ward, D.C. & Tattersall, P., eds), pp. 131-149, Cold Spring Harbor Laboratory, Cold Spring Harbor, NY.
14. Spalholz, B.A. & Tattersall, P. (1983). Interaction of minute virus of mice with differentiated cells: strain-dependent target cell specificity is mediated by intracellular factors. *J. Virol.* **46**, 937-943.
15. Segovia, J.C., Real, A., Bueren, J.A. & Almendral, J.M. (1991). *In vitro* myelosuppressive effects of the parvovirus minute virus of mice (MVMi) on hematopoietic stem and committed progenitic cells. *Blood* **77**, 980-988.
16. Kimsey, P.B., Engers, H.D., Hirt, B. & Jongeneel, C.V. (1986). Pathogenicity of fibroblasts and lymphocyte specific variants of minute virus of mice. *J. Virol.* **59**, 8-13.
17. Brownstein, D.G., Smith, A.L., Jacoby, R.O., Johnson, E.A., Hanser, G. & Tattersall, P. (1991). Pathogenesis of infection with a virulent allotropic variant of minute virus of mice and regulation of host genotype. *J. Clin. Invest.* **65**, 357-364.
18. Tattersall, P. & Bratton, J. (1983). Reciprocal productive and restrictive virus–cell interactions of immunosuppressive and prototype strains of minute virus of mice. *J. Virol.* **46**, 944-955.
19. Gardiner, E.M. & Tattersall, P. (1988). Mapping the fibrotropic and lymphotropic host range determinants of the parvovirus minute virus of mice. *J. Virol.* **62**, 2605-2613.
20. Ball-Goodrich, L.J. & Tattersall, P. (1992). Two amino acid substitutions within the capsid are coordinately required for acquisition of fibrotropism by the lymphotropic strain of minute virus of mice. *J. Virol.* **66**, 3415-3423.
21. Maxwell, I.H., Spitzer, A.L., Maxwell, F. & Pintel, D.J. (1995). The capsid determinant of fibrotropism for the MVMp strain of minute virus of mice functions via VP2 and not VP1. *J. Virol.* **69**, 5829-5832.
22. Tullis, G.E., Burger, L.R. & Pintel, D.J. (1993). The minor capsid protein VP1 of the autonomous parvovirus minute virus of mice is dispensable for encapsidation of progeny single-stranded DNA but it is required for infectivity. *J. Virol.* **67**, 131-141.
23. Ron, D. & Tal, J. (1985). Coevolution of cells and virus as a mechanism for the persistence of lymphotropic minute virus of mice during persistent infection in mouse L cells. *J. Virol.* **55**, 424-430.
24. Ron, D., Tattersall, P. & Tal, J. (1984). Formation of a host range mutant of the lymphotropic strain of minute virus of mice during persistent infection in mouse L cells. *J. Virol.* **52**, 63-69.
25. Horiuchi, M., Ishiguro, N., Goto, H. & Shinagawa, M. (1992). Characterization of the stage(s) in the virus replication cycle at which the host-cell specificity of the feline parvovirus sub-group is regulated in canine cells. *Virology* **189**, 600-608.
26. Truyen, U. & Parrish, C.R. (1992). Canine and feline host ranges of canine parvovirus and feline panleukopenia virus: distinct host cell tropisms of each virus *in vitro* and *in vivo*. *J. Virol.* **66**, 5399-5408.
27. Chang, S.F., Sgro, J.Y. & Parrish, C.R. (1992). Multiple amino acids in the capsid structure of canine parvovirus coordinately determine the canine host range and specific antigenic and hemagglutination properties. *J. Virol.* **66**, 6858-6867.
28. Truyen, U., Agbandje, M. & Parrish, C.R. (1994). Characterization of the feline host range and a specific epitope of feline panleukopenia virus. *Virology* **200**, 494-503.
29. Chapman, M.S. & Rossmann, M.G. (1995). Single-stranded DNA–protein interactions in canine parvovirus. *Structure* **3**, 151-162.
30. McKenna, R., Ilag, L.L. & Rossmann, M.G. (1994). Analysis of the single-stranded DNA bacteriophage ϕX174, refined at a resolution of 3.0 Å. *J. Mol. Biol.* **237**, 517-543.
31. Chen, Z., Stauffacher, C.V. & Johnson, J.E. (1990). Capsid structure and RNA packaging in comoviruses. *Sem. Virol.* **1**, 453-466.
32. Fisher, A.J. & Johnson, J.E. (1993). Ordered duplex RNA controls capsid architecture in an icosahedral animal virus. *Nature* **361**, 176-179.
33. Zlotnick, A., Natarajan, P., Munshi, S. & Johnson, J.E. (1997). Resolution of space group ambiguity and the structure determination of nodamura virus to 3.3 Å resolution from pseudo R32 (monoclinic) crystals. *Acta Cryst. D* **53**, 738-746.
34. Ban, N., Larson, S.B. & McPherson, A. (1995). Structural comparisons of the plant satellite viruses. *Virology* **214**, 571-583.
35. Hadfield, A.T., *et al.*, & Rossmann, M.G. (1997). The refined structure of human rhinovirus 16 at 2.15 Å resolution: implications for the viral life cycle. *Structure* **5**, 427-441.
36. Arnold, E. & Rossmann, M.G. (1990). Analysis of the structure of a common cold virus, human rhinovirus 14, refined at a resolution of 3.0 Å. *J. Mol. Biol.* **211**, 763-801.
37. Muckelbauer, J.K., *et al.*, & Rossmann, M.G. (1995). The structure of coxsackievirus B3 at 3.5 Å resolution. *Structure* **3**, 653-667.
38. Filman, D.J., Syed, R., Chow, M., Macadam, A.J., Minor, P.D. & Hogle, J.M. (1989). Structural factors that control conformational transitions and serotype specificity in type 3 poliovirus. *EMBO J.* **8**, 1567-1579.
39. Valegård, K., Murray, J.B., Stockley, P.G., Stonehouse, N.J. & Liljas, L. (1994). Crystal structure of an RNA bacteriophage coat protein–operator complex. *Nature* **371**, 623-626.
40. Llamas-Saiz, A.L., Agbandje-McKenna, M., Wikoff, W.R., Bratton, J., Tattersall, P. & Rossmann, M.G. (1997). Structure determination of minute virus of mice. *Acta Cryst. D* **53**, 93-102.
41. Jones, T.A., Zou, J.-Y., Cowan, S.W. & Kjeldgaard, M. (1991). Improved methods for building protein models in electron density maps and the location of errors in these models. *Acta Cryst. A* **47**, 110-119.
42. Chapman, M.S. & Rossmann, M.G. (1993). Structure, sequence and function correlations among parvoviruses. *Virology* **194**, 491-508.
43. Llamas-Saiz, A.L., Agbandje-McKenna, M., Parker, J.S.L., Wahid, A.T.M., Parrish, C.R. & Rossmann, M.G. (1996). Structural analysis of a mutation in canine parvovirus which controls antigenicity and host range. *Virology* **225**, 65-71.
44. Strassheim, M.L., Gruenberg, A., Veijalainen, P., Sgro, J.Y. & Parrish, C.R. (1994). Two dominant neutralizing antigen determinants of canine parvovirus are found on the threefold spike of the virus capsid. *Virology* **198**, 175-184.
45. Agbandje, M., Kajigaya, S., McKenna, R., Young, N.S. & Rossmann, M.G. (1994). The structure of human parvovirus B19 at 8 Å resolution. *Virology* **203**, 106-115.
46. Chipman, P.R., *et al.*, & Rossmann, M.G. (1996). Cryo-electron microscopy studies of empty capsids of human parvovirus B19 complexed with its cellular receptor. *Proc. Natl Acad. Sci. USA* **93**, 7502-7506.
47. Tattersall, P. & Cotmore, S.F. (1988). The nature of parvoviruses. In *Parvoviruses and Human Disease.* (Pattison, J.R., ed.), pp. 5-41, CRC Press, Boca Raton, FL.
48. Giranda, V.L., *et al.*, & Rueckert, R.R. (1992). Acid-induced structural changes in human rhinovirus 14: possible role in uncoating. *Proc. Natl Acad. Sci. USA* **89**, 10213-10217.
49. Cotmore, S.F., D'Abramo, A. & Tattersall, P.J. (1996). Aspects of the structure, assembly and unfolding of MVM particles revealed using anti-peptide antibodies. *Abstracts, American Society for Virology Meeting*, London, Ontario.
50. Li, Q., Yafal, A.G., Lee, Y.M., Hogle, J. & Chow, M. (1994). Poliovirus neutralization by antibodies to internal epitopes of VP4 and VP1 results from reversible exposure of these sequences at physiological temperature. *J. Virol.* **68**, 3965-3970.
51. Lewis, J.K., Bothner, B., Smith, T.J. & Siuzdak, G. (1998). Antiviral agent blocks breathing of the common cold virus. *Proc. Natl Acad. Sci. USA* **95**, 6774-6778.
52. Bothner, B., Dong, X.F., Bibbs, L., Johnson, J.E. & Siuzdak, G. (1998). Evidence of viral capsid dynamics using limited proteolysis and mass spectrometry. *J. Biol. Chem.* **273**, 673-676.
53. Barbis, D.P., Chang, S.F. & Parrish, C.R. (1992). Mutations adjacent to the dimple of the canine parvovirus capsid structure affect sialic acid binding. *Virology* **191**, 301-308.
54. Wu, H. & Rossmann, M.G. (1993). The canine parvovirus empty capsid structure. *J. Mol. Biol.* **233**, 231-244.
55. McPherson, A. (1982). *Preparation and Analysis of Protein Crystals.* Wiley & Sons, New York, NY.
56. Saenger, W. (1984). *Principles of Nucleic Acid Structure.* Springer-Verlag, New York, NY.
57. Kraulis, P. (1991). MOLSCRIPT: a program to produce both detailed and schematic plots of protein structures. *J. Appl. Cryst.* **24**, 946-950.
58. Chapman, M.S. (1993). Mapping the surface properties of macromolecules. *Protein Sci.* **2**, 459-469.
59. Smith, T.J. (1990). MacInPlot: a program to display electron density and atomic models on the Macintosh personal computer. *J. Appl. Cryst.* **23**, 141-142.